Gauge Field Induced Chiral Zero Mode in Five-Dimensional Yang Monopole Metamaterials

Shaojie Ma,[1,2] Hongwei Jia,[4] Yangang Bi,[1,5] Shangqiang Ning,[1] Fuxin Guan,[1] Hongchao Liu,[6] Chenjie Wang,[1] and Shuang Zhang[1,3,*]

[1]*New Cornerstone Science Laboratory, Department of Physics, The University of Hong Kong, Hong Kong 999077, China*
[2]*Shanghai Engineering Research Centre of Ultra Precision Optical Manufacturing, Department of Optical Science and Engineering, School of Information Science and Technology, Fudan University, Shanghai 200433, China*
[3]*Department of Electrical and Electronic Engineering, The University of Hong Kong, Hong Kong 999077, China*
[4]*Department of Physics and Institute for Advanced Study, The Hong Kong University of Science and Technology, Hong Kong 999077, China*
[5]*State Key Laboratory of Integrated Optoelectronics, College of Electronic Science and Engineering, Jilin University, 2699 Qianjin Street, Changchun 130012, China*
[6]*Institute of Applied Physics and Materials Engineering, University of Macau, Avenida da Universidade, Taipa, Macao SAR 999078, China*

(Received 2 February 2023; accepted 22 May 2023; published 15 June 2023)

Owing to the chirality of Weyl nodes characterized by the first Chern number, a Weyl system supports one-way chiral zero modes under a magnetic field, which underlies the celebrated chiral anomaly. As a generalization of Weyl nodes from three-dimensional to five-dimensional physical systems, Yang monopoles are topological singularities carrying nonzero second-order Chern numbers $c_2 = \pm 1$. Here, we couple a Yang monopole with an external gauge field using an inhomogeneous Yang monopole metamaterial and experimentally demonstrate the existence of a gapless chiral zero mode, where the judiciously designed metallic helical structures and the corresponding effective antisymmetric bianisotropic terms provide the means for controlling gauge fields in a synthetic five-dimensional space. This zeroth mode is found to originate from the coupling between the second Chern singularity and a generalized 4-form gauge field—the wedge product of the magnetic field with itself. This generalization reveals intrinsic connections between physical systems of different dimensions, while a higher-dimensional system exhibits much richer supersymmetric structures in Landau level degeneracy due to the internal degrees of freedom. Our study offers the possibility of controlling electromagnetic waves by leveraging the concept of higher-order and higher-dimensional topological phenomena.

DOI: 10.1103/PhysRevLett.130.243801

Singularities in momentum space, which emerge as low-energy excitations from a multifold degenerate spectrum, play a key role in topological physics [1,2]. For instance, a Weyl semimetal hosts Weyl points (WPs) in the momentum space, which support massless relativistic quasiparticles with quantized Chern numbers $c_1 = \pm 1$ [3–8]. Owing to this topological charge, its quantized Landau band structures under a magnetic field feature a single gapless chiral zero mode (CZM) [9–12], which underlies the celebrated chiral anomaly effect [13,14] and the negative longitudinal magnetoresistance [15].

Generalization of WPs to five-dimensional (5D) space leads to either zero-dimensional Yang monopoles (YMs) [16,17] or two-dimensional linked Weyl surfaces [18–22], both of which possess nontrivial second-order topology with second Chern number $c_2 = \pm 1$. These higher-dimensional singularities have been demonstrated in a metamaterial platform constructed by judiciously designed metallic helical structures, with three real momentum dimensions and two bianisotropic material parameters as synthetic dimensions [23,24]. Three-dimensional Fermi hypersurfaces and 1D Weyl arcs at the 4D boundary of the Yang monopole metamaterial (YMM) were observed, which are key signatures of the nontrivial c_2. Since YMs generalize WPs in higher dimensions with second-order topology, a natural question is how they would respond to a gauge field as a result of their nontrivial c_2 [25].

A series of recent papers [10,11,26–29] have shown that an artificial gauge field could be applied to a singularity by engineering the individual unit cell to shift the location of the degenerate point spatially. Such designs are excellent platforms for observing Landau levels and CZM induced by the interaction of quasiparticles and artificial external magnetic fields $\vec{B}$. However, limited by the available space-time dimensions, previous demonstrations have been limited to 2D or 3D systems. In this Letter, a 5D gauge field $\vec{A}$ is implemented by a judiciously designed inhomogeneous YMM with two synthetic dimensions represented by the

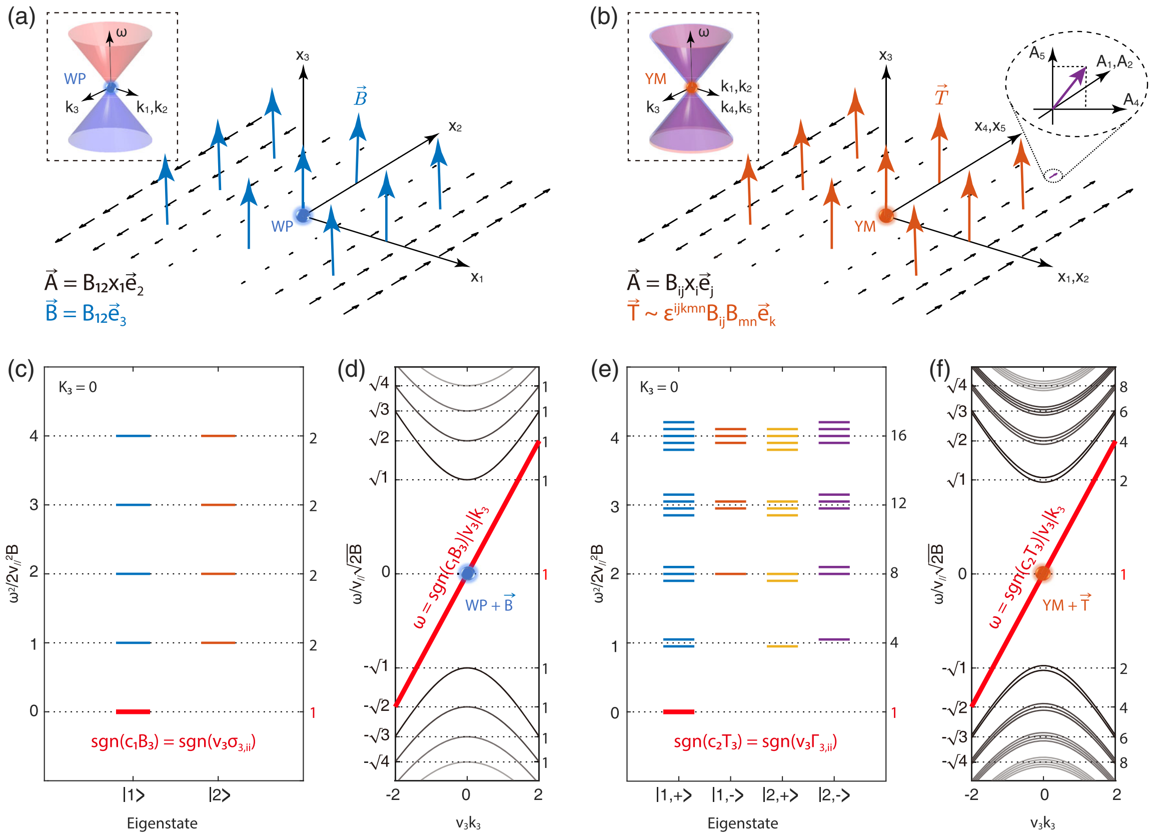

FIG. 1. Illustration of Landau Levels and CZM in WP and YM under a gauge field. (a) A WP in 3D space under an external magnetic field $\vec{B}$. (b) The counterpart of (a) in 5D space—a YM under an external 4-form pseudovector $\vec{T}$ field. The upper left insets in (a) and (b) show the linear dispersion spectrum near the singularity, and the upper right inset in (b) shows a 5D gauge field $\vec{A}$. (c) The supersymmetric Landau levels corresponding to the nonrelativistic squared WP Hamiltonian. (d) The dispersion spectrum of the relativistic WP Hamiltonian, with the red straight line representing the CZM. (e),(f) The counterpart of (c),(d) for YM, with two effective magnetic field components $B_{P1} \approx B_{P2}$. The numbers on the right-hand vertical axis indicate the degeneracy of each set of Landau levels if $|B_{P1}| = |B_{P2}|$.

antisymmetric bianisotropic terms. This gauge field indicates a 4-form background pseudovector field $\vec{T} \propto \vec{B} \wedge \vec{B}$ along the axial z direction, which matches the order of the differential form of nontrivial non-Abelian curvature $\vec{F} \wedge \vec{F}$ [30,31] induced by YM, where $\vec{F}$ is the 2-form Berry curvature and $\wedge$ is the wedge product. This non-Abelian curvature is mathematically equivalent to the tensor gauge field G_{1234} discussed in Ref. [32]. We for the first time experimentally demonstrate the existence of the generalized gapless CZM induced by the coupling between this pseudovector field $\vec{T}$ and the second Chern singularity in such a higher-dimensional second-order topological system.

We start with the comparison between WP and YM under a gauge field, as shown in Figs. 1(a) and 1(b). A typical WP is described by $H_{\mathrm{WP}} = \sum_{i=1}^{3} v_i k_i \sigma_i$, with σ_i the Pauli matrices. When coupled with a gauge field $\vec{A} = B_{ij}x_i\hat{e}_j$, by choosing an axis $\hat{e}_3$ along which the pseudovector magnetic field $\vec{B}$ is aligned, the corresponding magnetic field $\vec{B} = B_{12}\hat{e}_3 = B_3\hat{e}_3$ induces supersymmetric Landau levels in the nonrelativistic squared Hamiltonian:

$$H^2_{\mathrm{WP},G} = v_3^2k_3^2 + v_{\parallel}^2[(2n+1)|B_3| - \mathrm{sgn}(v_3)c_1B_3\sigma_z], \quad (1)$$

with n a non-negative integer [33]. The term $v_3^2k_3^2$ arises from the conserved axial wave vector k_3, with v_3 the corresponding Fermi velocity. For convenience, we set isotropic horizontal Fermi velocities $v_{i\neq 3} = v_{\parallel}$. The last term represents the Zeeman term induced by the magnetic field. Except for the zeroth mode, for every eigenstate of Weyl basis $|1\rangle$, there is always another counterpart eigenstate $|2\rangle$ with the same energy and a mode number difference of 1, as shown in Fig. 1(c). At $k_3 = 0$, due to the chiral symmetry $\{H_{\mathrm{WP}}, \sigma_3\} = 0$, these supersymmetric structures [33,34] indicate that for a WP under a gauge field there exist symmetric relativistic high-order Landau levels and a single CZM. The group velocity of one-way

CZM is determined by both the magnetic field B_3 and the chirality c_1 of WP:

$$\omega_{\mathrm{CZM}} = \mathrm{sgn}(c_1 B_3)|v_3|k_3, \tag{2}$$

as shown in Fig. 1(d) [10–12].

For a YM described by $H_{\mathrm{YM}} = \sum_{i=1}^{5} v_i k_i \Gamma_i$, with $\{\Gamma_i, \Gamma_j\} = 2\delta_{ij}$ satisfying the Clifford algebra, it has a globally doubly degenerate band structure and a fourfold degenerate point [16,17]. The system contains much richer internal structures due to a higher degree of freedom. In the presence of a 5D gauge field $\vec{A}$, in general, there exist ten 2-form magnetic field components B_{ij} and five 4-form pseudovector field components $T_k \propto \varepsilon^{ijkmn} B_{ij} B_{mn}$. By applying a coordinate transformation, one can reduce a uniform 2-form magnetic field to only two components $\{B_{P1}, B_{P2}\}$ individually operating on two separate sets of orthogonal 2-planes, which are both perpendicular to an axis $\hat{e}_3$ along which the pseudovector field $\vec{T}$ is aligned [see Sec. I in Supplemental Material (SM) [35]].

The presence of these fields leads to the following nonrelativistic squared Hamiltonian:

$$H^2_{\mathrm{YM},G} = \Sigma^2 \pm \sqrt{\Xi + c_2 T_3\, \mathrm{sgn}(v_3)\Gamma_3}, \tag{3}$$

where $\sum^2 = -\sum_j v_j^2 \mathcal{D}_j^2$ with $\mathcal{D}_j \equiv \partial_j - iA_j$, and $\Xi = \frac{1}{2}\sum_{i\neq j} v_i^2 v_j^2 B_{ij}^2$. In a proper Fock space, the two 2-form magnetic field components give rise to supersymmetric Landau levels in the nonrelativistic squared Hamiltonian:

$$\begin{aligned} H^2_{\mathrm{YM},G} = v_3^2 k_3^2 + v_\parallel^2 [&|B_{P1}|(2n_1+1) + |B_{P2}|(2n_2+1) \\ &- (|B_{P1}|\sigma_3 + |B_{P2}|\sigma_0) \otimes \tau_3], \end{aligned} \tag{4}$$

where $\{n_1, n_2\}$ are two non-negative integers, as shown in Fig. 1(e) with $B_{P1} \approx B_{P2}$ [33,38]. The generalized Zeeman term contains two sets of Pauli matrices, where σ and τ operate on the interband $|i\rangle$ and intraband $|\pm\rangle$ spaces, respectively. Because of the SO(5) rotation symmetry [39–41], the supersymmetric structure in the squared YM Hamiltonian possesses much richer degeneracies than its lower-dimensional counterpart—the WP, which possesses double degeneracy for all the nonzeroth modes. In the YM system, the degeneracy depends on the energy level, which will be $4N$ at the particular case $|B_{P1}| = |B_{P2}|$, with $N = n_1 + n_2 \neq 0$.

Importantly, there exists an individual CZM, as shown in Fig. 1(f). Interestingly, it is not the 2-form magnetic fields $\vec{B}$ but the 4-form pseudovector field $\vec{T}$ together with c_2 of the YM that finally determine the dispersion of CZM, with the direction of the group velocity given by

$$\omega_{\mathrm{CZM}} = \mathrm{sgn}(c_2 T_3)|v_3|k_3. \tag{5}$$

Here, the condition guarantees the same Zeeman lift direction in the interband space for the two constituent WPs. This generalized CZM is topologically protected by c_2. While useful for obtaining the dispersion of the CZM, this squared Hamiltonian cannot fully determine the eigenstates and topological properties. Hence, a more detailed equivalent lattice model in the Fock space is performed [12]. It is verified that the CZM is also protected by an equivalent topological invariant: a pair of opposite nested first Chern number $c_1|_{v_\pm}$ defined on the Wannier sectors [42–45] (see Secs. II and III in SM [35]).

In this work, we focus on this generalized CZM and verify its existence through microwave experiments of inhomogeneous metallic helical YMMs, as shown in Fig. 2. The designed YMM [23] has degenerate electric and magnetic resonances at the plasmonic frequency ω_p. Purely antisymmetric bianisotropic terms $\gamma_{xz} = -\gamma_{zx}$ and $\gamma_{yz} = -\gamma_{zy}$ serve as two synthetic wave vector dimensions k_4 and k_5, and purely antisymmetric tellegen terms $\varsigma_{ij} = -\varsigma_{ji}$ serve as shifts of three real wave vectors: $\Delta k_k = -\varepsilon_{ijk}\omega_p \varsigma_{ij}$ (see Sec. IV in SM [35]). A periodic metamaterial [23] just behaves like a 5D YM with fourfold degeneracy located at $[\vec{K}_{\mathrm{YM}}, \omega_p]$, in which the space of Clifford operators Γ_i is spanned by two degenerate longitudinal plasma modes $\{|E_z\rangle, |H_z\rangle\}$ with flat dispersion and two transverse electromagnetic modes $\{|E_x\rangle, |E_y\rangle\}$ [brown lines in Fig. 2(d)].

For an inhomogeneous metamaterial, following the rules of minimal coupling $\partial_j \mapsto \mathcal{D}_j \equiv \partial_j - iA_j$ in the usual covariant derivative argument, a vector gauge field $\vec{A}$ can be viewed as a space-dependent shift of the YM locations $\vec{K}_{\mathrm{YM}}(\vec{r})$ in the 5D momentum space, with magnetic field $B_{ij} = i \cdot [\mathcal{D}_i, \mathcal{D}_j] = \partial_i A_j - \partial_j A_i$ caused by this spatial shift [46]. Without loss of generality, we choose the axial direction along the z direction. Therefore, the inhomogeneous YMM slow varying in the xy plane can introduce an arbitrary nontrivial gauge field $\vec{A}(\vec{r}) = A_i(x,y)\hat{e}_i$ by designing the space-dependent magnetoelectric tensor [47]. Compared with the homogeneous system, this inhomogeneous system not only introduces the magnetic fields B_{ij} that can couple with the first-order topological singularity, but also contains a nontrivial 4-form field component $T_3 = \frac{1}{4} v_\parallel^4 \cdot \vec{B} \wedge \vec{B} \cdot \hat{e}_3 = 2v_\parallel^4 (B_{15}B_{24} - B_{14}B_{25} + B_{12}B_{45})$ along the z direction, which interacts with the second-order topological singularity of the YM and induces the generalized CZM in 5D photonic YMM.

Figure 2(a) shows a schematic diagram for a specific inhomogeneous YMM with only nonzero B_{15}, B_{24} and all other $B_{ij} = 0$. The shift of the YM only occurs in the synthetic dimensions by varying the bianisotropy terms: $A_4 = -\omega_p \gamma_{xz}(\vec{r}) = B_{24} y$ and $A_5 = -\omega_p \gamma_{yz}(\vec{r}) = B_{15} x$, which correspond to two individual space-dependent mass terms in three real dimensions [48,49]. Note that such a

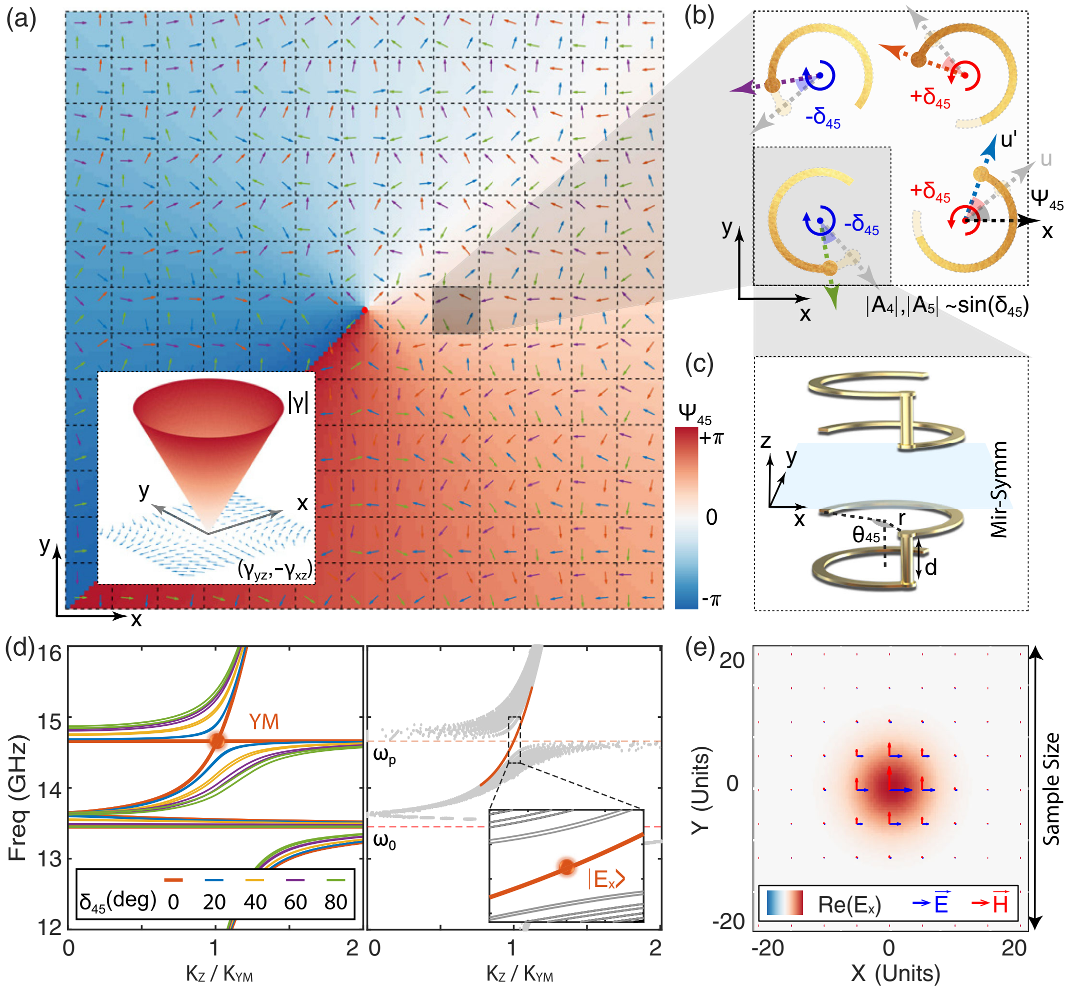

FIG. 2. Illustration of Inhomogeneous Yang metamaterial. (a)–(c) The configuration of an inhomogeneous YMM with $A_4 = B_{24}y$ and $A_5 = B_{15}x$. The inset in (a) represents the magnitude and angle distribution of the bianisotropy vectors, and the color map labels the spatial distribution of ψ_{45}. (b),(c) The top view and side view of the metallic helices, respectively. The spatial distribution of the two angles δ_{45} and ψ_{45} is precisely designed to achieve an arbitrary gauge field distribution. (d) The local (left) and global (right) dispersion of the designed inhomogeneous metamaterial along the axial direction k_z. The brown line represents the dispersion of the original YM (left) and CZM (right). (e) The field distribution of CZM at the original YM location.

configuration does not require any tellegen materials for observing the CZM. The space-dependent bianisotropy distribution is realized by a set of rotated metallic helical units, as shown in Figs. 2(b) and 2(c). In each unit, four precisely adjusted helical structures combined with their mirror counterparts are collectively rotated to the angles $\Phi_{1\mapsto 4} = \psi_{45} + [+\delta_{45}, +\delta_{45} + 90°, -\delta_{45} + 180°, -\delta_{45} + 270°]$, which can realize purely antisymmetric bianisotropic terms satisfying $\gamma_{xz} + i\gamma_{yz} \propto \sin\delta_{45} \exp[i(\psi_{45} + 45°)]$ [23]. Therefore, $\vec{A}(\vec{r})$ can be realized in this inhomogeneous photonic metamaterial through an appropriate spatial distribution of rotation angles $[\delta_{45}, \psi_{45}]$. In the experimental demonstration, we design $\sin\delta_{45}$ to be linearly varying with radius, which varies from 0 to 1 through 20 units, and a space-dependent phase distribution $\psi_{45} = \mathrm{atan2}(x, y) - 45°$. This inhomogeneous YMM contains a uniform effective magnetic flux density $B_{15} = B_{24} \approx -1210\ \mathrm{m}^{-2}$ generated by the spatially shifted $\vec{A}(\vec{r})$ and a uniform 4-form pseudovector field $T_3 \approx (0.011\omega_p)^4$ along the z direction, which opens up a sufficiently large enough band gap of approximately 0.39 GHz (see Sec. IV in SM [35]).

The local (left-hand panel) and global (right-hand panel) dispersions of this metamaterial are shown in Fig. 2(d). Locally, a nonzero angle δ_{45} behaves like an effective mass, which opens a band gap and constructs two pairs of degenerate bands near YM. Meanwhile, globally this inhomogeneous metamaterial supports a single E_x-polarized confined state near the original YM, which is the CZM induced by the nontrivial field T_3 and protected by c_2. This eigenstate corresponds to a localized zero-order Hermite-Gauss field distribution, as shown in Fig. 2(e). Thus, a polarization-dependent dispersion spectrum can be measured to verify this CZM.

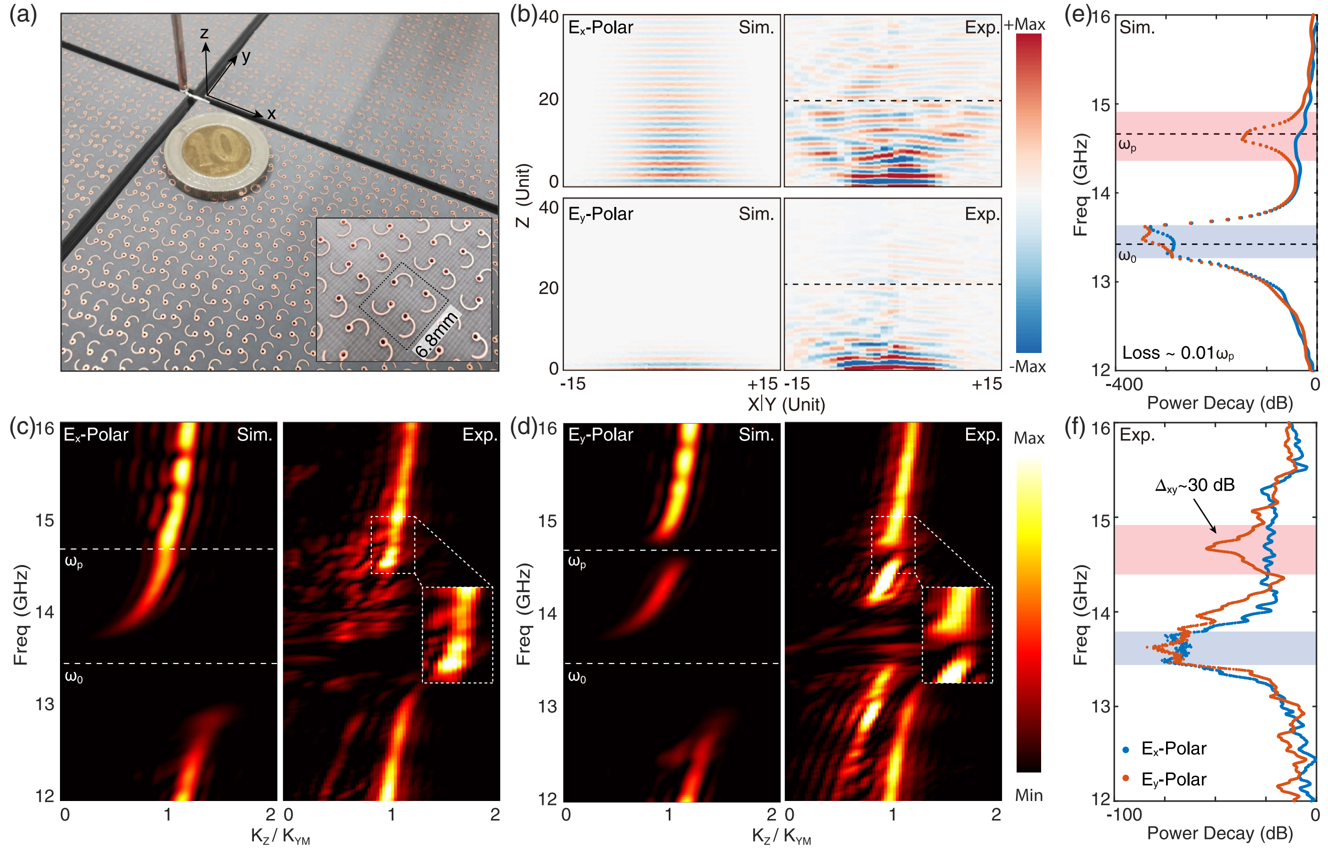

FIG. 3. Experimental observation of the polarization-dependent dispersion of the 5D CZM. (a) Photograph of the top surface of the sample, fabricated with printed circuit board technology, with one unit cell indicated by the black square. Two 3-mm-wide vertical slits are cut through the center of the sample to measure the field distribution inside the metamaterial. (b) The simulated (left) and measured (right) electric field distribution in the slits by different polarized excitations at the plasma frequency. The data $z \in (0, 20)$ units and $z \in (20, 40)$ units are from two independent measurements. (c),(d) The simulated (left) and measured (right) dispersion spectra by (c) E_x-polarized and (d) E_y-polarized excitations. In both cases, the direction of the probe antenna is aligned to the polarization of the wave launched by the horn antenna, and E_x/E_y polarization is detected in the XZ/YZ slit, respectively. (e),(f) The (e) simulated and (f) measured transmitted power for different polarizations obtained from integration along the corresponding slit. The K_{YM} positions of the experimental data are normalized individually.

The sample is constructed by stacking up 160 printed circuit board layers (40 unit cells along the z direction), as shown in Fig. 3(a). A linearly polarized wave is launched by a horn antenna located below the center of the bottom layer, while the field distribution inside the vertical slits is detected by the near-field scanning of a monopole antenna aligned to a copolarization direction. Figure 3(b) shows the simulated and measured copolarization field distribution at the plasma frequency around 14.66 GHz in different polarization setups. The E_x-polarized field can propagate through the metamaterial, while the E_y-polarized field decays rapidly along the z direction, agreeing with our theoretical prediction that this inhomogeneous metamaterial supports a single E_x-polarized CZM, but behaves as a band gap for the E_y-polarized excitation. A significant contrast about 30 dB between different polarizations is observed in the measured transmitted power near the plasma frequency, as shown in Figs. 3(e) and 3(f). The dispersion spectra of the two polarizations along k_z, obtained through Fourier transformation of the field patterns, show a significant difference near the plasma frequency from about 14.55 to 14.71 GHz, both in simulation and in the experiment, as shown from the comparison between Figs. 3(c) and 3(d). Such difference in dispersion spectrum between the two polarizations is consistent across a series of measurements at different in-plane locations. In comparison, the dispersion spectrum and transmitted power are both nearly polarization independent at frequencies away from the plasma frequency (see Sec. V in SM [35] for experimental details). This contrast provides direct evidence for the presence of polarized zeroth mode near YM.

In summary, we have explored the interaction of higher-order topological singularities with a gauge field in a 5D system, and we experimentally demonstrated the existence of CZM by employing an inhomogeneous metamaterial platform. Under a gauge field, the YMs with nontrivial c_2 provide a much richer Landau structure than its 3D counterpart, due to the interplay between 2-form magnetic fields $\vec{B}$ and 4-form pseudovector fields $\vec{T}$. Interestingly, the formation of the CZM directly results from the interaction between c_2 and the pseudovector $\vec{T}$ field, which serves as a new manifestation of the intriguing topological properties of YM. Our work provides new approaches for electromagnetic control by exploiting the combination of higher-dimensional topology and artificially engineered gauge fields.

This work was supported by the Research Grants Council of Hong Kong (AoE/P-701/20, 17309021, 16307621), the New Cornerstone Science Foundation, and the start-up funding of Fudan University (JIH1232082Y). We would like to thank Professor T. T. Luu for his help in sample preparation.

The authors declare no conflict of interest.

*Corresponding author.
shuzhang@hku.hk

[1] X. Wan, A. M. Turner, A. Vishwanath, and S. Y. Savrasov, Phys. Rev. B **83**, 205101 (2011).
[2] N. P. Armitage, E. J. Mele, and A. Vishwanath, Rev. Mod. Phys. **90**, 015001 (2018).
[3] L. Lu, L. Fu, J. D. Joannopoulos, and M. Soljačić, Nat. Photonics **7**, 294 (2013).
[4] S.-Y. Xu *et al.*, Science **349**, 613 (2015).
[5] L. Lu, Z. Wang, D. Ye, L. Ran, L. Fu, J. D. Joannopoulos, and M. Soljačić, Science **349**, 622 (2015).
[6] B. Q. Lv *et al.*, Phys. Rev. X **5**, 031013 (2015).
[7] A. A. Burkov, Nat. Mater. **15**, 1145 (2016).
[8] B. Yang *et al.*, Science **359**, 1013 (2018).
[9] H. B. Nielsen and M. Ninomiya, Phys. Lett. **130B**, 389 (1983).
[10] H. Jia, R. Zhang, W. Gao, Q. Guo, B. Yang, J. Hu, Y. Bi, Y. Xiang, C. Liu, and S. Zhang, Science **363**, 148 (2019).
[11] V. Peri, M. Serra-Garcia, R. Ilan, and S. D. Huber, Nat. Phys. **15**, 357 (2019).
[12] Y. X. Zhao and S. A. Yang, Phys. Rev. Lett. **126**, 046401 (2021).
[13] Q. Li, D. E. Kharzeev, C. Zhang, Y. Huang, I. Pletikosić, A. V. Fedorov, R. D. Zhong, J. A. Schneeloch, G. D. Gu, and T. Valla, Nat. Phys. **12**, 550 (2016).
[14] J. Gooth *et al.*, Nature (London) **547**, 324 (2017).
[15] J. Xiong, S. K. Kushwaha, T. Liang, J. W. Krizan, M. Hirschberger, W. D. Wang, R. J. Cava, and N. P. Ong, Science **350**, 413 (2015).
[16] C. N. Yang, J. Math. Phys. (N.Y.) **19**, 320 (1978).
[17] S. Sugawa, F. Salces-Carcoba, A. R. Perry, Y. Yue, and I. B. Spielman, Science **360**, 1429 (2018).
[18] B. Lian and S. C. Zhang, Phys. Rev. B **94**, 041105(R) (2016).
[19] K. Hashimoto, X. Wu, and T. Kimura, Phys. Rev. B **95**, 165443 (2017).
[20] B. Lian and S. C. Zhang, Phys. Rev. B **95**, 235106 (2017).
[21] J. Y. Chen, B. Lian, and S. C. Zhang, Phys. Rev. B **100**, 075112 (2019).
[22] K. Hashimoto and Y. Matsuo, Phys. Rev. B **101**, 245138 (2020).
[23] S. Ma, Y. Bi, Q. Guo, B. Yang, O. You, J. Feng, H.-B. Sun, and S. Zhang, Science **373**, 572 (2021).
[24] S. Ma, B. Yang, and S. Zhang, Photonics Insights **1**, R02 (2022).
[25] X. L. Qi, T. L. Hughes, and S. C. Zhang, Phys. Rev. B **78**, 195424 (2008).
[26] A. G. Grushin, J. W. F. Venderbos, A. Vishwanath, and R. Ilan, Phys. Rev. X **6**, 041046 (2016).
[27] D. I. Pikulin, A. Chen, and M. Franz, Phys. Rev. X **6**, 041021 (2016).
[28] A. Westström and T. Ojanen, Phys. Rev. X **7**, 041026 (2017).
[29] H. Jia, R.-Y. Zhang, W. Gao, S. Zhang, and C. T. Chan, Phys. Rev. B **104**, 045132 (2021).
[30] A. Roy and P. Bandyopadhyay, J. Math. Phys. (N.Y.) **30**, 2366 (1989).
[31] H.-U. Yee and P. Yi, Phys. Rev. D **101**, 045007 (2020).
[32] K. Hasebe, Nucl. Phys. **B886**, 952 (2014).
[33] K. Hasebe, Int. J. Mod. Phys. A **31**, 1650117 (2016).
[34] M. Bellec, C. Poli, U. Kuhl, F. Mortessagne, and H. Schomerus, Light Sci. Appl. **9**, 146 (2020).
[35] See Supplemental Material at http://link.aps.org/supplemental/10.1103/PhysRevLett.130.243801 for supporting data and detailed information about the experiments, which includes Refs. [35,36].
[36] M. Erdoğdu and M. Özdemir, Math. Sci. Appl. E **8**, 1 (2020).
[37] A. Perez-Gracia and F. Thomas, Adv. Appl. Clifford Algeb. **27**, 523 (2016).
[38] Y. Li, S. C. Zhang, and C. Wu, Phys. Rev. Lett. **111**, 186803 (2013).
[39] K. Hasebe, Nucl. Phys. **B920**, 475 (2017).
[40] K. Hasebe, Nucl. Phys. **B956**, 115012 (2020).
[41] K. Hasebe, Phys. Rev. D **105**, 065010 (2022).
[42] W. A. Benalcazar, B. A. Bernevig, and T. L. Hughes, Science **357**, 61 (2017).
[43] W. A. Benalcazar, B. A. Bernevig, and T. L. Hughes, Phys. Rev. B **96**, 245115 (2017).
[44] M. Lohse, C. Schweizer, H. M. Price, O. Zilberberg, and I. Bloch, Nature (London) **553**, 55 (2018).
[45] I. Petrides and O. Zilberberg, Phys. Rev. Res. **2**, 022049(R) (2020).
[46] M. E. Peskin, *An Introduction to Quantum Field Theory* (CRC Press, 2018).
[47] V. S. Asadchy, A. Díaz-Rubio, and S. A. Tretyakov, Nanophotonics **7**, 1069 (2018).
[48] X. Gao, L. Yang, H. Lin, L. Zhang, J. Li, F. Bo, Z. Wang, and L. Lu, Nat. Nanotechnol. **15**, 1012 (2020).
[49] L. Yang, G. Li, X. Gao, and L. Lu, Nat. Photonics **16**, 279 (2022).